ELSEVIER

Contents lists available at ScienceDirect

Progress in Organic Coatings

journal homepage: www.elsevier.com/locate/porgcoat





Effect of molecular weight on polymer solution facilitated transfer of non-Brownian particles

Bashir Khoda a,*, William Gramlichb, S.M. Naser Shovona, Ibrahim Khalila

- a Department of Mechanical Engineering, The University of Maine, Orono, ME, United States of America
- ^b Department of Chemistry, The University of Maine, Orono, ME, United States of America

ARTICLE INFO

Keywords:
Particle transfer
Polymer content
Viscous layer
Polydisperse particle

ABSTRACT

Solution driven particle transfer on solid substrates has many industrial applications but can be difficult to control and characterize. In this study, poly(methyl methacrylate) (PMMA) is considered as the binder polymer, and the effect of the molecular weight (MW) on particle transfer through entrainment is investigated. The transfer phenomenon of polydisperse spherical rigid micro-particles from the PMMA solution has been analyzed and two hypotheses are tested here: (i) there exists a threshold polymer content below which only the smallest particles will be transferred from the bulk; (ii) at the same viscosity of different molecular weight PMMA solution, the solid transfer phenomenon will be similar. By changing the mass and viscosity using three PMMA samples with different MWs in the 1,3-dioxolane solvent, we observe low, intermediate, and high viscous regimes of the PMMA-dioxolane solution system. The low, intermediate, and high viscous regimes can be controlled with the MW and can entrain distinct particle size distributions onto surfaces. This behavior is thoroughly analyzed and relates to the film formation. These results confirmed our first hypothesis that we could use polymer content to control the particle size distribution and that a threshold polymer content exists. However, at similar viscosities, higher molecular weight polymers yielded lower average particle sizes and narrower distributions, which is counter to our second hypothesis. These findings can provide a better understanding of the binder behavior and its influence on the particle transfer process which opens-up the possibility of particle sorting process from a polydisperse suspension mixture and high-yield material transfer for porous structure coating and joining processes. Understanding the particle transfer process can also enable reverse engineering of the liquid carrier system in a complex mixture, which can be beneficial for industrial applications.

1. Introduction

Solution driven thin-film formation on solid substrates is undergoing continuous development and is widely used in many industrial applications [1–3]. Thin films are applied for the production of sensors [4–7], nano-coating for hydrophobic surfaces [8], particle filtration [9,10], batteries [11], fuel cells [12], and optical displays [13–15]. This film formation process can be carried out either directly using physical processes or indirectly using chemical and electrochemical reactions [16]. A wide range of film thickness (nanometer to micrometer) can be achieved from these processes by changing their process parameters [17–21]. Dip-coating is a simple and facile for the film formation over a plate, fiber, and irregular shaped object. Materials are transferred at the solid-liquid interface during the withdrawal of the substrate from the suspension [22]. The thickness of the polymer film for a non-

evaporating solution formed over the substrate was first predicted by Landau and Levich and then Derjaguin which is known as the famous LLD equation [23,24]. The thickness of the polymer film, in their work, is dependent on the withdrawal speed (U) of the substrate from the suspension, the viscosity of the suspension (η), and the capillary length $l_c = \sqrt{\gamma/\rho g}$, where γ and ρ are the surface tension and density of the fluid respectively and g is the acceleration with respect to gravity. The entrainment regime is dependent on the capillary number $Ca = \eta U/\gamma$ which is denoted as the ratio of the viscous force and surface tension force. For a small capillary number ($Ca < 10^{-2}$), the thickness of the polymer film is determined by the competition between the viscous force and surface tension force only, and the LLD equation for thickness is $h = 0.94 l_c Ca^{2/3}$. On the other hand, at larger capillary numbers, gravity is dominant over the surface tension force which leads the equation of thickness to be $h = l_c Ca^{1/2}$ and due to the gravitational

E-mail address: bashir.khoda@maine.edu (B. Khoda).

^{*} Corresponding author.

drainage, a non-uniform layer thickness is observed over the substrate [25]. The relevant parameter to predict the film thickness over the cylindrical substrate is $Go = R/l_c$ [26]; where R is the radius of the cylindrical substrate and l_c is the capillary length. The modified LLD equation to calculate the film thickness over fiber for Go < 3 is determined as $h = 1.34RCa^{2/3}$ [27,28]. Thus, the film thickness from a dilute solution is a well-studied phenomenon in literature.

The generated film can often be used as a delivery vehicle for solid transfer (i.e., nano- or micro- particles) on a flat, cylindrical, or complex substrate. In such circumstances, a polymer solution is used as the liquid carrier solution (LCS), where the immiscible particles are added resulting in a slurry, suspension, or heterogeneous mixture [9,29,30]. The simple but effective dip coating technique is often the popular choice for the LCS based delivery technique and the transferred particles are directly related to the characteristics of the film. The film thickness over the substrate can be controlled from few nanometers to hundreds of micrometers with relative ease by changing the dip coating process parameters [31]. Colosqui and Morris [32] numerically showed that the required film thickness should be greater than the particle diameter (h >a; where a is particle diameter). However, Sauret et al. [33] experimentally demonstrated that a thin film can hold particles of six times larger than the liquid film thickness. Gans et al. [25] measured the average liquid film thickness while coating with silicone oil. They showed the liquid film thickness remains constant over a range of withdrawal speeds depending upon the diameter of the particle used in the suspension. They found the average liquid film thickness is 20-30 μm between 0.02 and 0.1 mm/s withdrawal speed for the 20 μm particles and the film thickness is 100-150 µm between 0.05 and 1 mm/s withdrawal speed for the 140 µm particles. In another work on dipcoating, Dincau et al. [34] showed the variation of non-dimensional liquid film thickness capillary number at different fiber radius and viscosity of the silicone oil. In one of our previous articles [30] we experimentally showed that the critical liquid film thickness for particle entrainment is h=0.16a for 6.5 % binder and h=0.26a for 10.5 % binder, when the micro-particles were a significantly higher specific density than the LCS.

The existing model can predict the film thickness of the polymer solution accurately before drying. Additionally, the film formation and solid transfer process is often characterized based on solvent evaporation [35,30], rheology of the LCS [3,36], solid loading of transferable particles [37], and particle size distribution [38,39]. The molecular weight of polymers is another defining characteristic which determines the solution properties of polymer chains as well as their capability to sterically stabilize particles [40,41]. Molecular weight controls the length of the polymer chain which controls the viscosity of the suspension. However, the effect of polymer molecular weight on polymer film formation and the resultant solid transfer phenomenon is scarce in literature. In a limited experiment [42], change in viscosity is reported with concentration or % w/v of a light emitting polymer (LEP) in solution. However, the relationship between the molecular weight and the film thickness for the LEP polymer is inconclusive in that investigation. In this study, poly(methyl methacrylate) (PMMA) is considered as the binder polymer, and the effect of the MW on dense micro-particle entrainment is investigated during dip coating. The polydisperse spherical rigid micro-particles transfer phenomenon from the PMMA solution has been analyzed to determine how the PMMA film facilitates particle transfer. Two hypotheses were tested: (i) there exists a threshold polymer content below which only the smallest particles will be transferred from the bulk; (ii) at the same viscosity of different molecular weight PMMA solutions, the solid transfer phenomenon will be similar.

2. Materials and methodology

The liquid carrier system (LCS) consisted of 1,3-dioxolane as solvent and poly(methyl methacrylate) (PMMA) as the binder, both procured from Sigma Aldrich, USA. To observe the effect of the molecular weight

of the binder on the film formation and particle transfer, we used three different molecular weights: 15000 (15 K), 120,000 (120 K), and 350,000 (350 K) Da. These molecular weights were reported by the supplier to be weight average molecular weights (Mw) measured by size exclusion chromatography (SEC). The molecular weight distributions were also analyzed by us using SEC on an Agilent 1260 Infinity instrument with three Phenogel (Phenomenex) columns in series with pore sizes 50, 10³, and 10⁶ Å, and a refractive index detector calibrated with linear polystyrene standards. The mobile phase was tetrahydrofuran (THF) at a flow rate 1.0 mL min⁻¹ with a column and detector temperature of 35 $^{\circ}$ C. This SEC analysis yielded M_{w} and dispersity (Θ) values for each sample. The density of the solvent and the binder for the LCS were 1.06 g/cm³ and 1.17 g/cm³, respectively, at room temperature (RT = 25 °C) as provided by the supplier. A magnetic stirrer was used overnight to dissolve the binder at different weight percentages in the solvent. The dissolution of the binder was confirmed by a dynamic light scattering (DLS) experiment in the LCS solution. With the increase in molecular weight of the polymer, the size of the polymer chain and the hydrodynamic volume of the chains in solution increases resulting in higher viscosities [43]. The LCS solution was transparent and provided clear visualization of particles in it. The viscosity was measured by an Anton Paar MCR 302 Rheometer applying a flow curve test using a 50 mm diameter parallel plate with a 0.2 mm gap filled with sample.

Brazing powder (Nicrobraz LM; procured from Wall Colmonoy company, Ohio; Spherical dia range $\sim 0\text{--}100~\mu\text{m}$) was used as solid inorganic particles which were added into the LCS. The particles were sorted using a Gilson Performer III shaker through Stainless Steel 635 Mesh (20 μm) in our lab to reduce polydispersity. After sieving, the reduced particles were imaged using SEM and analyzed for their particle size using ImageJ. The average particle size of the distribution was 7.56 \pm 3.98 μm and the particle density was 7.97 g/cm³. AISI 1006 mild steel cylindrical rod with an average diameter of 1.06 mm (procured from ClampTite LLC) was used as the dipping substrate. An ultrasound bath filled with acetone was used for 10 min at 50 °C to remove the passive film over the rod substrate.

Solid particles in the LCS mixture created a density imbalance which facilitated the sedimentation and separation in the mixture. External kinetic energy in the form of agitation was provided to counteract the gravitational force of the particles by using a magnetic stirrer at 750 rpm and it created a uniform distribution of particles in the LCS, acting as pseudo-suspension. An in-house custom made dip coating setup was used for all the experiments as described in one of our previous articles [3]. During the experiments, the immersion time was 10 s and the withdrawal speed was 20 mm/s. When the substrate was inserted into the suspension, a thin film of PMMA and solvent was created over the substrate and particles were entrained on the substrate. The entrained particles and their size will depend upon the characteristics of this PMMA film. After dipping, the solid substrates were dried in an oven and images were captured using VHX 7000 Digital 4 K microscope (KEY-ENCE corp.) for further analysis. The influence of MW at the same viscosity was analyzed by measuring the solvent evaporation following similar experimental protocols. A 23 μL droplet of LCS solution of same viscosity (4 mPa.s) at different MW (15 K, 120 K and 350 K) of PMMA was placed on a glass slide. The droplet mass was measured every 30 min for a total of 180 min.

The characteristics of the transferred particles from the image was important to analyze but challenging due to the lack of contrast between substrate surface and particle. Due to the deep drawing fabrication of the metal rod, a rough and irregular surface morphology is common (Fig. 1-b & c). After entrainment of the particles, it created a heterogeneous image of the particle-substrate (HIPS) system. The pixel contrast between particle and substrate in HIPS was difficult to differentiate with existing image analysis tools (e.g., ImageJ, variable thresholding) and they generated significant error in particle analysis without labor intensive semantic knowledge-based post processing. To address these challenges, a deep learning object detection algorithm based on YOLOv5

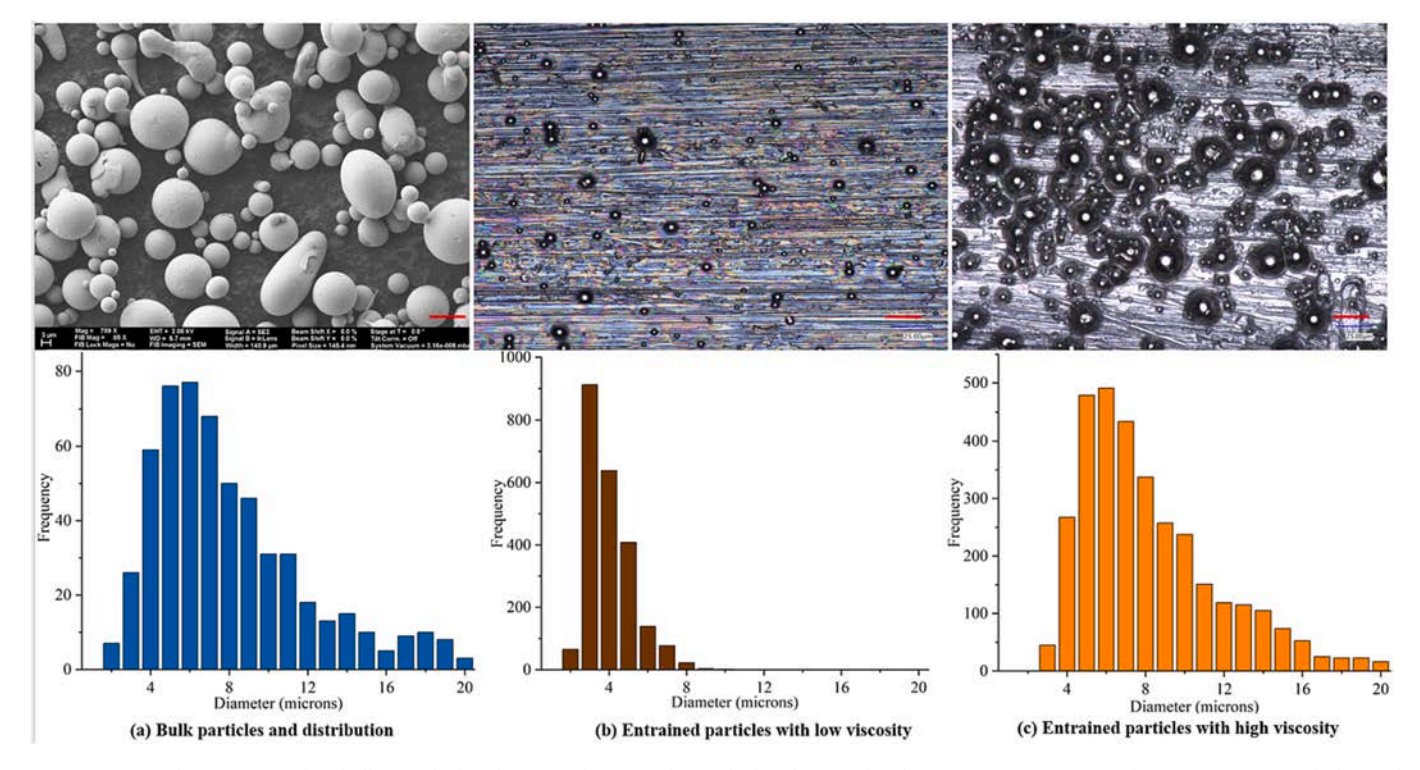


Fig. 1. Images and comparison of (a) bulk particle distribution and entrained particle distribution after dip coating in PMMA-Dioxolane (LCS) system with (b) 120 k PMMA low (0.92 mPa s) and (c) 15 k PMMA high (6.05 mPa s) LCS viscosity. Scale bar is 25 μm.

has been developed in our prior work [44] and used here to analyze the entrained particles. The developed artificial intelligence based automated computational tool has demonstrated >97 % accuracy for identifying and analyzing the polydisperse particles in HIPS. Three locations (bottom, middle and top) along the dipped rod were selected for imaging and three pictures were taken in each location. Thus, a total nine images were used as the datasets for each composition to analyze the transferred particles size distribution and surface coverage (Table 1).

3. Results

3.1. Characterizing the liquid viscosity and evaporation

The liquid carrier solution was prepared by mixing the solvent with polymeric binder at different concentrations. The molecular weight (MW) of polymers and the polymer concentration both work to resist the solvent flow. High MW polymers exhibit a long molecular chain that

enhances the intermolecular interactions which resists solvent flow and increases the viscosity. Moreover, at higher concentration more polymer molecules (chains) exist causing overlaps and entanglement within the solution space which reduces the mobility and increases the viscosity [45]. In this work, the influence of both the MW and concentration variation have been discussed in relation to the particle transfer mechanism. Three different MW of PMMA (15 K, 120 K and 350 K) were used in the polymer solution at different PMMA volume fraction and the viscosity of the LCS was measured with a rheometer. A predictive model was generated with polynomial curves fitting for each molecular weight by assuming that the concentrations were sufficiently dilute and the polymer were dissolved in a good solvent enabling use of Huggin's equation for viscosity [46]. Thus, a quadratic equation reasonably fit the data ($R^2=0.99$) for estimating the viscosity at different MW of PMMA as shown in Fig. 2.

The 1,3-dioxolane is an evaporative solvent and the generated dry film thickness clearly depends upon the evaporation characteristics of

Table 1 Composition of suspension mixture, viscosity, and particle size.

Molecular wt.	Solution viscosity (mPa.s)	PMMA weight (g)	Particle vol %	Solvent vol %	PMMA vol %	PMMA wt %	Average particle size (µm)	Capillary number, <i>Ca</i>	Particle count/ mm ²
15 K MW	0.72	0.06	10	89.28	0.72	0.46	4.61 ± 2.33	5.47×10^{-4}	443
PMMA	0.75	0.15	10	88.21	1.79	1.15	3.75 ± 1.56	5.71×10^{-4}	913
	0.81	0.22	10	87.31	2.69	1.74	3.62 ± 1.35	6.19×10^{-4}	395
	1.91	0.58	10	83.07	6.93	4.45	6.68 ± 2.76	1.5×10^{-3}	1942
	3.99	1.12	10	76.55	13.45	8.60	7.31 ± 3.06	2.98×10^{-3}	3353
	6.05	1.33	10	74.03	15.97	10.19	7.77 ± 3.68	4.43×10^{-3}	3276
120 K MW	0.92	0.06	10	89.28	0.72	0.46	3.46 ± 1.17	7.00×10^{-4}	2265
PMMA	1.46	0.15	10	88.21	1.79	1.15	5.42 ± 3.11	$1.11 imes 10^{-3}$	1710
	1.91	0.19	10	87.71	2.29	1.47	5.04 ± 1.71	1.52×10^{-3}	2101
	2.04	0.22	10	87.31	2.69	1.74	4.11 ± 1.99	1.55×10^{-3}	1630
	3.99	0.42	10	84.94	5.06	3.26	5.81 ± 2.19	3.02×10^{-3}	2184
	6.05	0.58	10	83.03	6.97	4.48	6.82 ± 3.18	4.52×10^{-3}	2516
350 K MW	1.91	0.06	10	89.28	0.72	0.46	4.70 ± 1.11	1.53×10^{-3}	5318
PMMA	3.99	0.15	10	88.21	1.79	1.15	4.94 ± 2.84	3.04×10^{-3}	3575
	6.05	0.22	10	87.31	2.69	1.74	5.70 ± 2.80	4.56×10^{-3}	4020

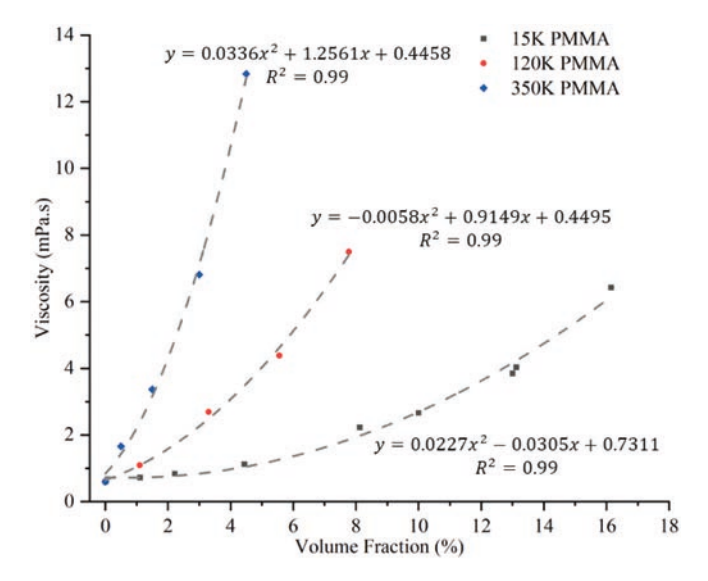


Fig. 2. Predictive viscosity of liquid carrier system (LCS) by polynomial fitting of the measured data points.

the solvent during and after the dip coating process. In our prior work [30], we observed that the measured film thickness of 15 K PMMA was lower than the theoretical thickness derived from the LLD equation. We also observed that the solvent evaporation rate becomes slower with the increase of binder concentration and viscosity due to a formation of a viscous top layer of PMMA. The remaining solvent after evaporation is plotted against time in Fig. 3 using the technique discussed in the methodology section. For the same viscosity, the 15 K PMMA had a slightly lower evaporation rate compared to 120 K and 350 K PMMA due to the higher concentration of polymer at 15 K to reach the same viscosity as the other polymer solutions. This finding follows the evaporation theory of polymer solution discussed in Geng et al. [47]. Higher concentration of polymer provides more resistance for solvent evaporation which results in relatively higher viscous layer thickness that accumulates more polymer molecules on the surface of the substrate.

3.2. Solid loading and pseudo suspension

The addition of rigid particles on the LCS solution modifies it to a phase separated mixture due to their high specific-density difference (~8 times). The external kinetic energy provided by a magnetic stirrer at just-suspending-speed helps the particles rotate continuously and evenly throughout the LCS solution which transforms it to a pseudo suspension. Suspensions with different volume fractions of particles have been divided into three regimes: dilute ($\phi_p \leq 0.01 \sim 0.02$), semi-dilute ($\phi_p \leq$ 0.25), and concentrated ($\phi_p > 0.25$) where ϕ_p is the particle volume fraction [36]. A suspension in the dilute regime is considered as a Newtonian fluid and in the concentrated regime it is a non-Newtonian fluid. In the semi-dilute regime, the suspension behaves approximately like a Newtonian fluid. Gilbert et al. identified Newtonian behavior on glass bead suspension of 80 μ m to 100 μ m particle diameter at $\phi_p =$ 34.3% [36]. Also, Pasquino et al. [48] observed Newtonian behavior PMMA spheres (\sim 14 μm dia.) in polyisobutylene and polydimethylsiloxanes carrier suspensions for a volume fraction ranging from 2 % to 10 %. In this work, the particle volume fraction, $\phi_p = 10\%$ was added to the LCS to create the pseudo suspension which was assumed to be a Newtonian fluid. Also, no coagulation was observed in the mixture, confirming their non-Brownian behavior.

4. Discussion

4.1. Expected viscosity behavior

The rheology of the LCS varies depending on the MW or concentration variation of polymer. Einstein provided a linear relationship between solid loading and viscosity for dilute suspension. This relationship can be extended to polymer solutions considering the polymer coil as an impenetrable sphere through which the solvent is unable to flow [49]. Thus, the viscosity (η) of dilute polymer solution can be expressed as a function of polymer concentration:

$$\eta = \eta_s(1 + c[\eta]) \tag{4}$$

where η_s is the viscosity of the solvent, c is the polymer concentration, and $[\eta]$ is the intrinsic viscosity. The expected viscosity (η) of polymer solution is plotted as a function of polymer concentration, c, in Fig. 4 considering the linear relationship of Eq. (4). The higher concentrations

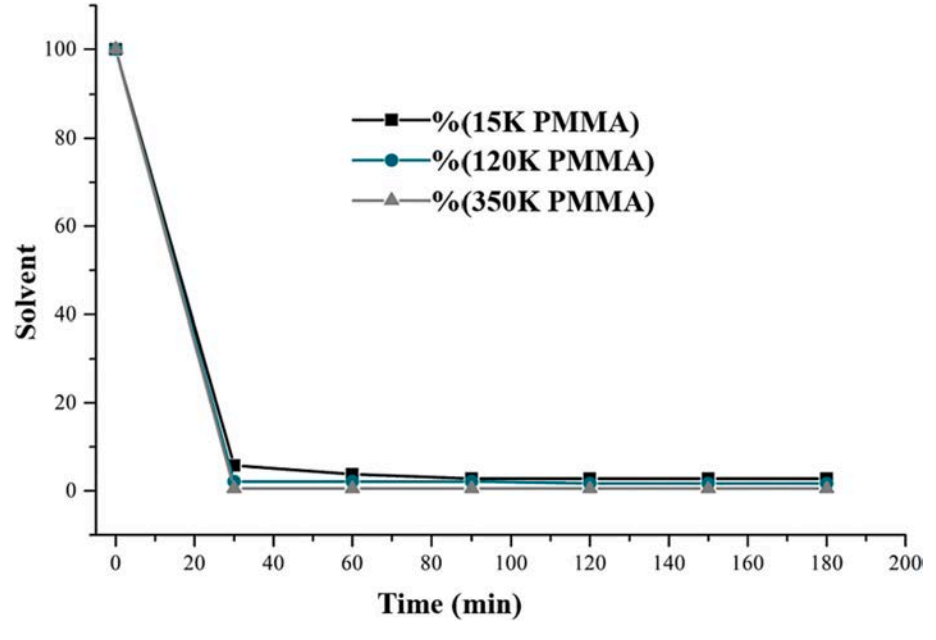


Fig. 3. Solvent evaporation as a function of time at different MW polymer solution.

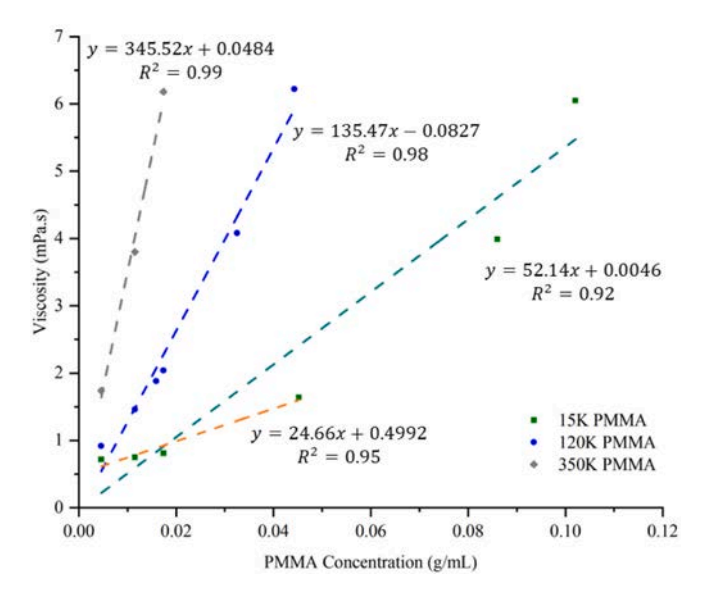


Fig. 4. Viscosity as a function of concentration for 350 K (diamond), 120 K (circle), and 15 K (square) PMMA in solution over the entire sample range. The orange curve represents only dilute regime of 15 K PMMA with higher R² value.

the 15 K PMMA deviate from linearity, suggesting non-dilute solutions at higher concentrations.

After considering the dilute conditions below 0.05 g/mL of 15 K PMMA, a more linear trend with higher $\rm R^2$ valued is plotted on Fig. 4. This reveals that several concentrations for 15 K PMMA cannot be considered dilute conditions and should follow a higher degree expression as:

$$\eta = \eta_s (1 + c[\eta] + k_H c^2 [\eta]^2)$$
 (5)

where k_H is the Huggins coefficient, which is a measure of excluded volume effects due to polymer solvent interactions [50]. These interactions become more significant at higher concentrations and the solution will behave differently from dilute conditions at higher concentrations. Considering only the dilute regime or linearity, the intrinsic viscosity $[\eta]$ can be calculated using the slopes in Fig. 4. The solvent viscosity η_s is provided by the supplier as 0.59 mPa.s and the calculated intrinsic viscosity $[\eta]$ for each molecular weight is reported in Table 2. The intrinsic viscosity is a function of molecular weight following the Mark-Houwink equation [51], expressed as:

$$[\eta] = kM^a \tag{6}$$

where k and a are constants. To perform a more accurate analysis using Eq. 6, the weight average molecular weight ($M_{\rm w}$) was measured by SEC (Table 2). The measured values for the 15 K and 350 K agreed well with the supplier reported value, but, interestingly, the 120 K sample appeared to have a significantly lower $M_{\rm w}$ than reported. This deviation may be due to the supplier for this sample using significantly different SEC analysis conditions for their analysis than the other samples. From the data in Table 2, the parameters are calculated to be a=0.84 and $k=0.016 \frac{ml}{g} \left(\frac{mol}{g}\right)^{0.84}$. A theoretical ratio of the intrinsic viscosities for different molecular weights using this Mark-Houwink equation implies

Table 2Intrinsic viscosity and measured molecular weight data of different molecular weight of PMMA in 1,3-dioxolane.

PMMA	M _w (kDa)	Ð	Measured intrinsic viscosity (mL/g)
15 K	16	2.3	42.0
120 K	49	4.8	227
350 K	320	1.7	588

that the 350 K PMMA has 4.8 and 12 times higher intrinsic viscosity than the 120 K and 15 K PMMA samples. Similarly, the 120 K sample has 2.6 times higher intrinsic viscosity than 15 K PMMA. We hypothesize that any differences in particle size, distribution and surface coverage can be attributed to the variation of intrinsic viscosity and resultant polymer content in the LCS solution which is discussed in this section.

4.2. Formation in low viscosity regime

While the substrate is pulled out from the suspension, a thin liquid film is formed on the substrate. The liquid film provides the viscous drag force and particles entrain on the substrate when the viscous drag force becomes larger than the resistive capillary force. This liquid film contains the polymer binder and entrapped solvent which is influenced by the viscosity of LCS solution and the concentration of binder present. When the viscosity of LCS remains low (~ 1 mPa.s), the solvent evaporation becomes faster due to the thin polymer shell and a relatively thinner film forms on the substrate. Similarly, solutions with low binder content have a high evaporation rate and results in a thin liquid film which cannot provide enough binding strength for larger particles due to minimal contact area. Therefore, large particles are dragged down easily from the substrate and a mono-disperse (narrow size range) particle distribution can be observed as shown in Figs. 5 and 6. Only particles less than $\sim 10 \, \mu m$ are observed in this low viscosity regime. For example, a 120 K PMMA LCS solution with 0.92 mPa s viscosity exhibits particle entrainment ranging from 2 μm and 10 μm with an average of 3.46 μm diameter. At 0.81 mPa s viscosity of 15 K PMMA LCS solution provides particle entrainment from 2 µm to 9 µm with an average of 3.62 µm diameter. Interestingly, at low viscosity (< 1 mPa s), the number of entrained particles per unit area are significantly lower (<1000 particles/mm²) than at viscosity values above 1 mPa s in most circumstances (except for 120 K PMMA \approx 2265/mm², which may be due to its higher dispersity) as presented in Table 1. This phenomenon may be attributed to only the smallest particles being possibly entrapped and excluding the larger particles of the bulk particle distribution (Fig. 1a). Therefore, the 15 K molecular weight polymer in this regime is too small to efficiently entrap particles at this lower concentration.

4.3. Transformation to the high viscosity regime

When the viscosity of the LCS solution increases, larger particles tend to adhere on the liquid film than the low viscosity regime due to higher film thickness. Between 1 mPa s to 2 mPa s viscosity, the size distribution of accumulated polymers started shifting towards mixed ranges (monoand poly-disperse) at different MW of polymer binder. For example, an almost monodisperse (narrow size range) and polydisperse (original bulk distribution) particle distribution can be observed with 350 K and 15 K PMMA at ~2 mPa s viscosity, respectively. However, 1.46 mPa s and 2 mPa s of 120 K PMMA shows an intermediate (between monodisperse and polydisperse) distribution of particles as shown in Figs. 5 and 6. The distribution also shows that significantly more smaller particles are entrained than larger particles (left skewed). The different behavior the 120 K PMMA compared to the other two samples may be due to the higher dispersity of this polymer sample leading to wider range of molecular weight influences (Table 2). Additionally, this phenomenon can be explained by a polymer content effect. For a similar viscosity, a lower molecular weight polymer will have higher polymer content (% wt) as compared to the higher molecular weight polymer. As a result, 15 K will have the highest polymer content in the LCS solution resulting in a lower relative evaporation rate and a thicker dry film than 120 K and 350 K materials. This helps entrain both smaller and larger particles and the distribution becomes close to the bulk distribution. Alternatively, 350 K has the least amount of polymer content resulting in a higher relative evaporation rate and thinner dry film than 120 K and 15 K. However, for 120 K PMMA, the intermediate polymer content entrained both small and large particles. Since, the distribution shows a

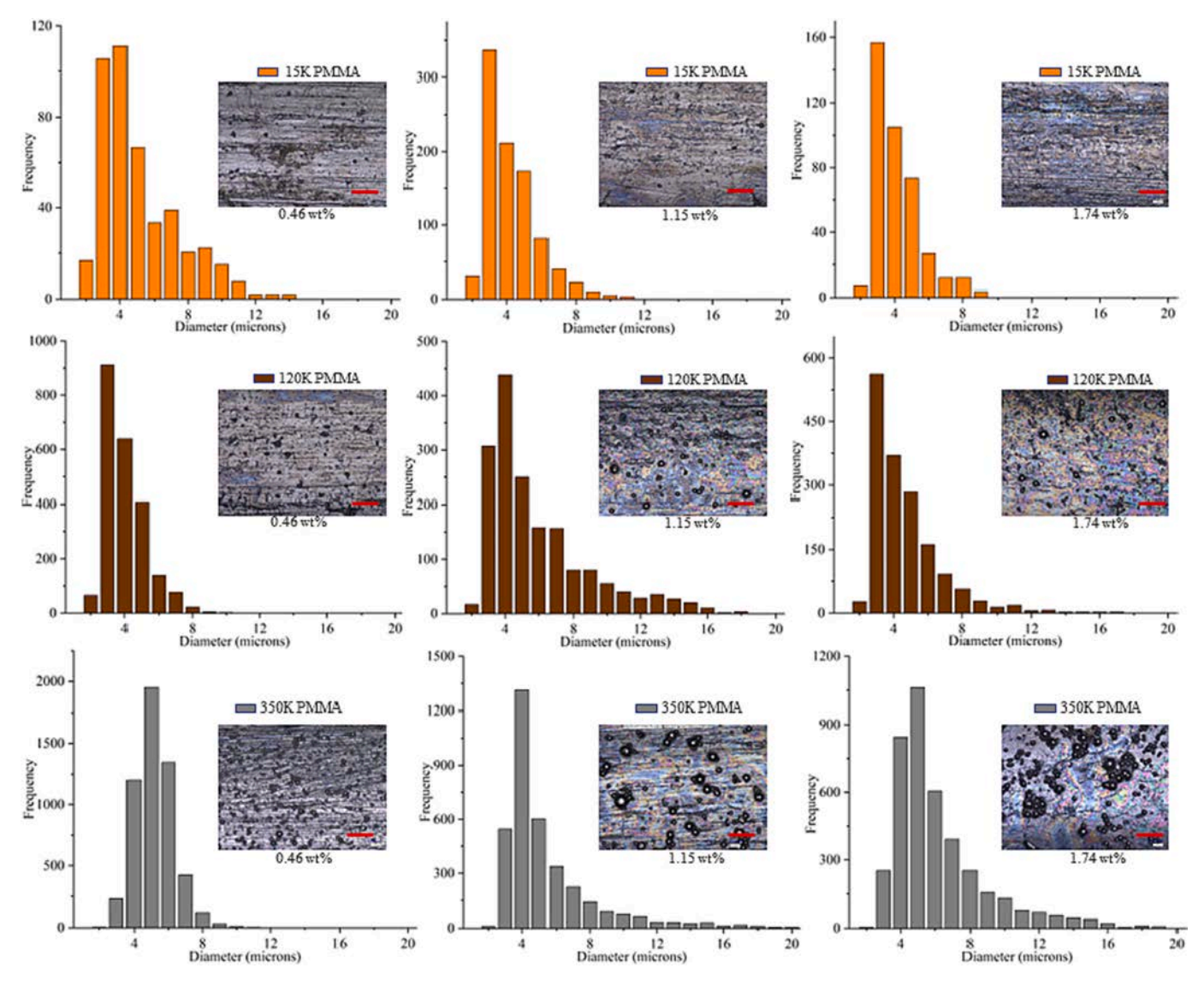


Fig. 5. Comparison of particle size distributions for LCS with the same wt% PMMA down a column. Scale bar is $50~\mu m$.

higher number of smaller than larger particles (skewed left), this composition (120 K and $\sim\!1.46$ mPa s) may have the threshold film thickness value for larger (>10 $\mu m)$ particles or the broad molecular weight distribution may lead to effects from large and small polymers and not only the average MW. Similarly, the threshold film thickness for 15 K PMMA is between 0.81 mPa s and 1.91 mPa s. Interestingly, at this transformative viscosity range (1–2 mPa s) of the PMMA-dioxolane system, the number of entrained particles per unit area is close to 2000/mm² except for the 350 K PMMA ($\approx\!5318/mm^2$) as presented in Table 1. This different behavior for the 350 K PMMA could possibly be due to entrapment of the small particles to the surface when submerged because of a larger interfacial region of adsorbed polymer.

4.4. High viscosity regime

When the LCS viscosity becomes higher than 2 mPa.s, all of the LCS solutions with different MW of PMMA entrained polydisperse particles size distributions (bulk distribution), except for 350 K, as shown in Figs. 5 and 6. For the 350 K polymer, a monodisperse particle distribution can still be observed at 1.91 mPa.s and the distribution is polydisperse at 3.99 mPa.s in our experiment. Thus, the large particle threshold viscosity for 350 K is between 1.91 mPa.s and 3.99 mPa.s, which are higher viscosities than 120 K and indicates that the large

particle threshold is molecular weight dependent. Since the molecular weight affects viscosity, maintaining the viscosity at different molecular weights require different polymer contents. At higher viscosities, during drying the polymer shell is thicker because of higher polymer concentrations, which reduces solvent evaporation and increases the liquid film thickness. With a greater liquid film thickness, entrained particles have more contact area and a higher binding strength during entrainment. For example, both 15 K and 120 K PMMA yield the entire bulk particle distribution by entraining large particles, which is possible since they have a high enough concentration of polymer to exceed the threshold film thickness for large particle entrainment. However, around 2 mPa.s LCS viscosity, the 350 K PMMA yields a narrow particle distribution of smaller particles because it has a lower concentration of polymer which increases the solvent evaporation and reduces the liquid film thickness as compared to the 15 K and 120 K PMMA of same viscosity. This thin liquid film remains below the threshold value for large particle entrainment and cannot provide enough strength to adhere large particles.

4.5. Effect of LCS viscosity and polymer content on surface coverage

The LCS solution viscosity is mainly driven by the variation of the MW of PMMA and its concentration. When the viscosity is similar for

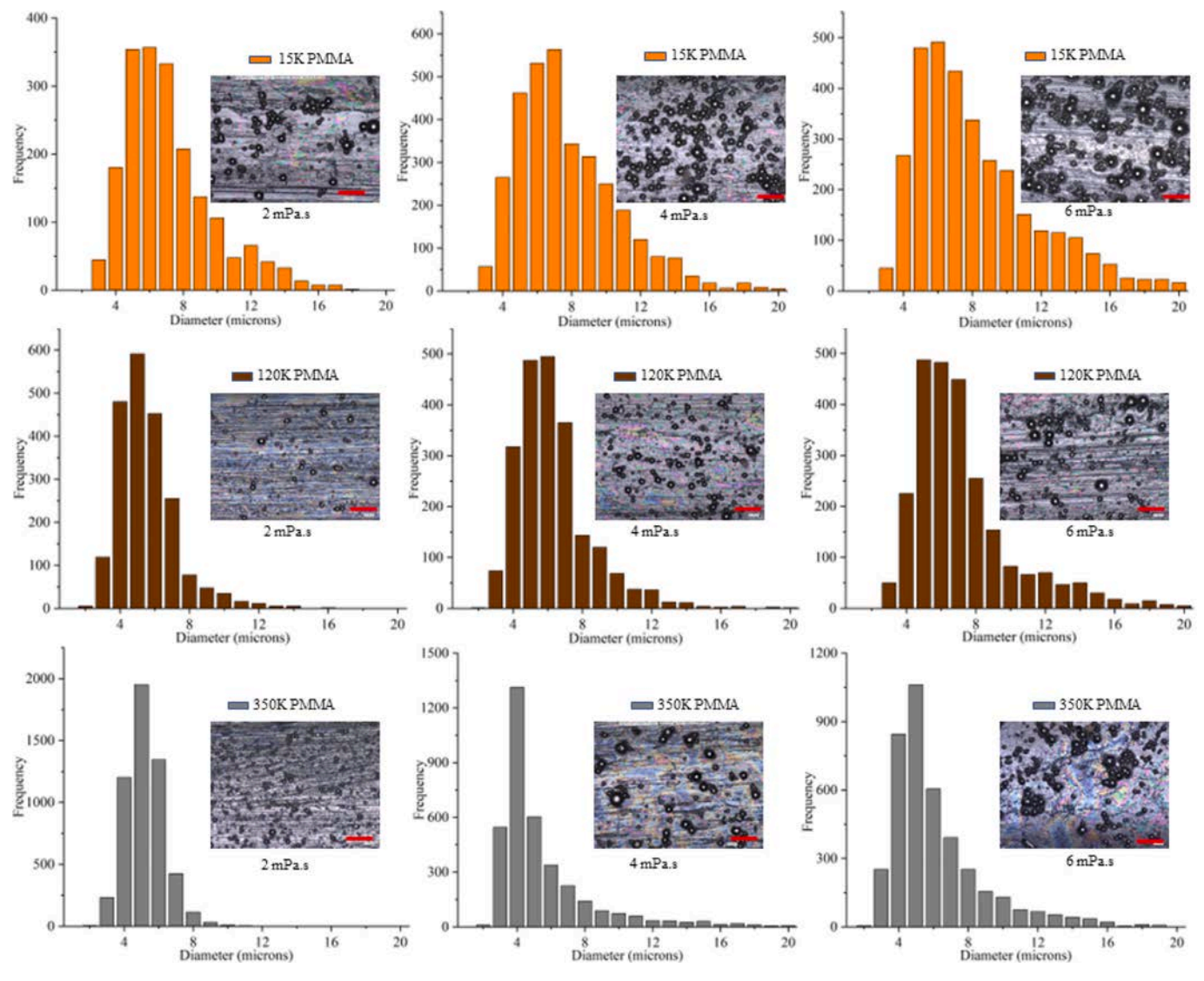


Fig. 6. Comparison of the particle size distributions for LCS with similar viscosities down a column. Scale bar is $50~\mu m$.

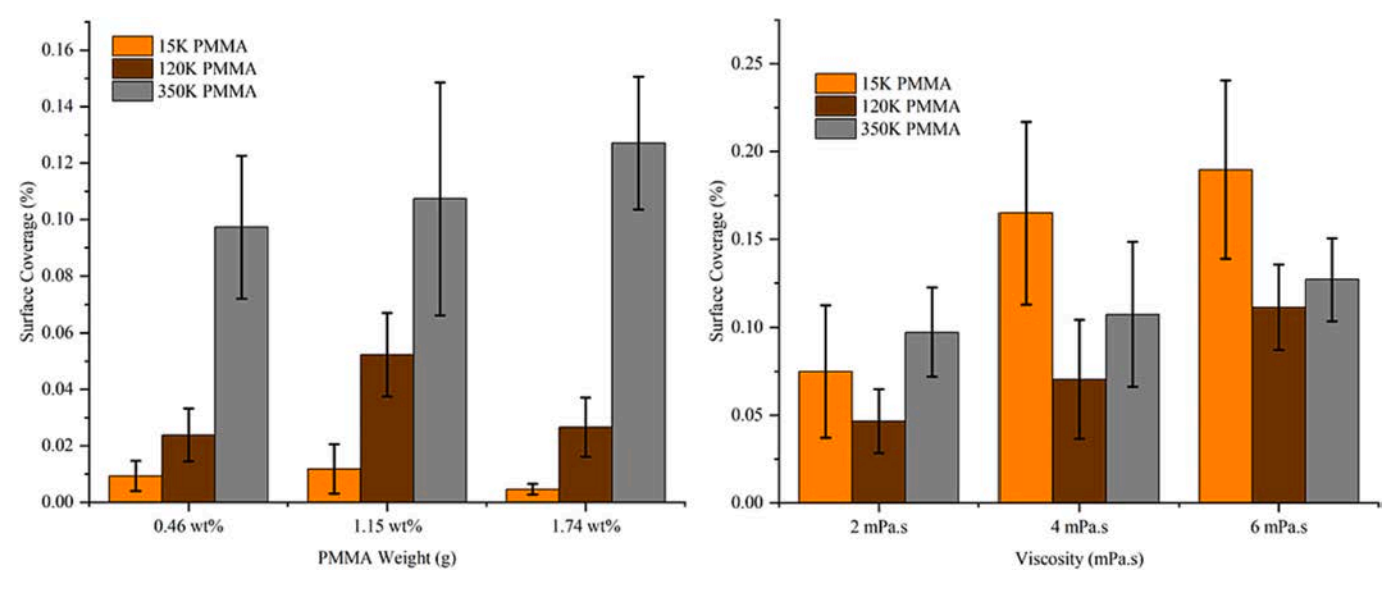


Fig. 7. Surface coverage at (left) similar weight of PMMA and (right) similar viscosity of LCS.

different MWs, more polymer is required for a low MW polymer at the same volume of LCS mixture. High polymer content tends to reduce the mobility of solvent flow. For LCS solutions with similar viscosities, 15 K has the maximum polymer content and it resists the solvent evaporation more, forming a thicker liquid and dry film on the substrate. Therefore, more particles adhere in the liquid film covering more surface area than the high MW counterpart, which has a lower polymer content at a similar viscosity. Also, for a higher viscosity and polymer content, the liquid film is thicker which helps large particles adhere in the liquid film limiting the gravitational effect. Therefore, in the high viscous regime, larger particles are entrained on the substrate, covering more surface area. These phenomena can be observed in all compositions in the dilute polymer content regime. It should be noted that at 4 and 6 mPa s using the 15 K PMMA are not in the dilute (linear) regime as indicated in Fig. 4. This concentrated regime will create different flow behaviors, independent of viscosity. The increased polymer-polymer interactions in the non-dilute regime could lead to a more gel-like behavior, slowing particle movement relative to the dilute system. For example, comparing samples with 6 mPa s viscosity, the 350 K PMMA suspension yields smaller particles (avg. dia. 5.7 µm) and lower surface coverage (12.7 %) due to a thinner film. In contrast, the 15 K PMMA suspension at 6 mPa s captures large particles (avg. dia. 7.77 µm) and more surface coverage is achieved on the substrate (19 %) shown in Fig. 7 due to its high concentration of polymer.

In the similar polymer weight experiments, the polymer content remained fixed in the LCS solution, but the viscosity varied with the change of polymer MW. At the same polymer content, high MW polymer in LCS solution yields higher viscosity and the polymer layer resists the evaporation of solvent, yielding a thicker liquid and dry film. This liquid film facilitates transfer of all sizes of particles and limits gravitational effects. Thus, the surface coverage as well as the particle size increased with the higher viscosity. For example, at 1.74 wt% of the different MW polymer in the LCS, the 15 K PMMA has the lowest viscosity (0.81 mPa s) and it yields only 0.46 % coverage of particles with an average particle diameter of 3.62 µm. However, the 350 K PMMA LCS has a higher viscosity (6.05 mPa s), and it provides significantly higher surface coverage (12.7 %) than the similar weight of 15 K PMMA suspension. The significant jump in surface coverage at same PMMA mass loading (Fig. 7a) can be also explained by the Mark-Houwink relationship. The 350 K PMMA has 2.3 times higher intrinsic viscosity than 120 K and 8.9 times higher intrinsic viscosity than 15 K PMMA, which will lead to the additional surface coverage that is visible at all the same mass loading values in Fig. 7. Moreover, the similar weight samples are all in the dilute polymer regime, so their particle size is dictated by viscosity of the polymer solutions and the amount of polymer in the solution. Low polymer content leads to smaller particles because they are small enough to adhere to the surface with little polymer 'glue' while the

larger particles cannot adhere.

When the cumulative size distribution of similar weight and similar viscosity samples is compared to the bulk particle, in Fig. 8, a systematic shifting of the particle size distribution can be observed. For a similar viscosity, 80 % of all entrained particles are $<\!10\,\mu m$ in the dilute regime of the LCS. However, the concentrated gel-like samples of 15 K at 4 and 6 mPa s viscosity showed almost similar distribution like bulk particles. In similar weight samples, the cumulative particle size distribution is shifted towards left side compared to bulk distribution reducing the average particle size since all these LCS samples are in the dilute regime because of the low polymer concentration in the LCS.

The variation of polymer MW and its mass loading changes the viscosity as well as capillary number, (Ca) of the pseudo suspension. As the particle concentration is constant ($\phi_p=10\%$) and the concentration of polymer changes with their MW, the capillary number varies with the viscosity changes which can be presented with Krieger & Dougherty equation, described in our previous work [30]. At a similar viscosity of the LCS, the capillary numbers remain close to each other for different MW of polymer although the polymer mass loading varies. This variation of polymer mass loading results in different particle sizes entrained, which is independent of capillary number as shown in Fig. 9. In general, at the same capillary number, the average particle size decreases with increasing PMMA MW. For example, at a Ca of 3×10^{-3} the 350 K PMMA has an average particle size of 4.94 μ m whereas the 15 K PMMA

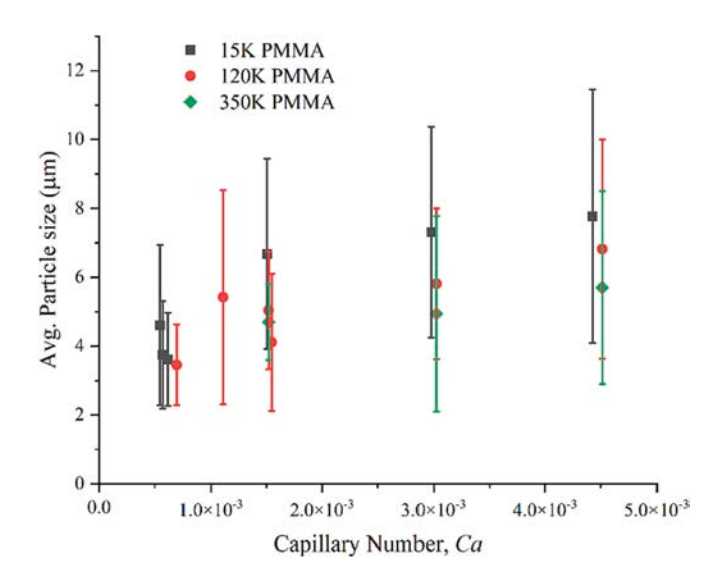


Fig. 9. Avg. particle size as a function of Capillary Number (*Ca*) for different molecular weight (MW) PMMA.

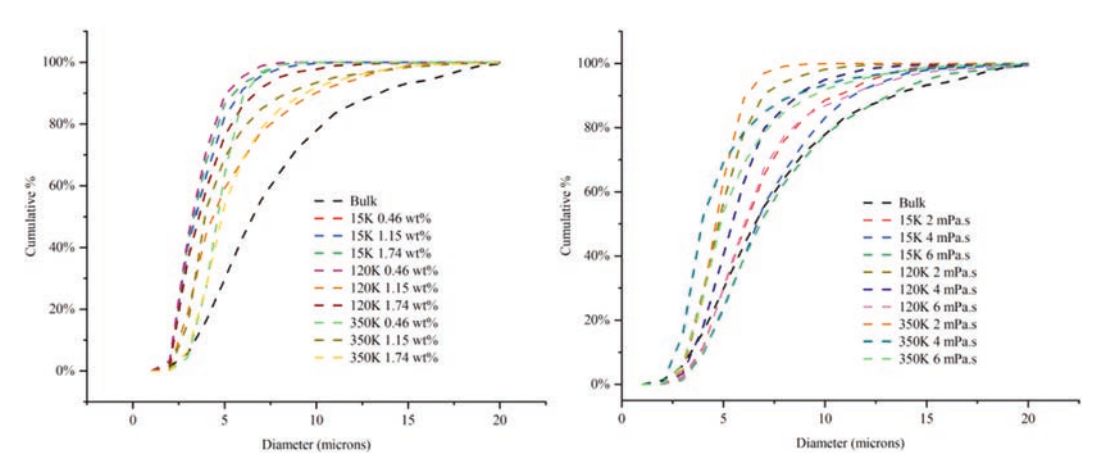


Fig. 8. Cumulative size distribution comparison with bulk particles at similar weight (left) and similar viscosity (right).

has higher average particle size of $7.31~\mu m$ closer to the bulk particle size ($7.56~\mu m$). This analysis further supports that the liquid film thickness due to solvent evaporation rate and the dry film thickness due to total polymer content can be used to control the particle size. Furthermore, by using the higher MW PMMA, less polymer can be used to achieve the same results as a lower molecular weight polymer.

5. Conclusions

In this paper, the entrainment of solid, high-density micro-particles using three different MW of PMMA in a LCS mixture was investigated to understand the influence of polymer binder on the solid transfer process. For the LCS solution, the effects of polymer mass loading and polymer MW was certainly visible on the particle size, distribution, and surface coverage. In experiments, the samples with <2 mPa s viscosity showed dilute solution behavior which resulted in smaller particle size distribution compared to the bulk particles. However, for 4 mPa s and 6 mPa s viscosities of 15 K samples, the solution followed a concentrated gel-like behavior and yielded a similar particle size distribution as the bulk particles which is independent of the viscosity of pseudo suspension. These results confirmed our first hypothesis that we could use polymer content to control the particle size distribution and that a threshold polymer content exists. However, at similar viscosities, higher molecular weight polymers yielded lower average particle sizes and narrower distributions, which is counter to our second hypothesis. This behavior was attributed to higher evaporation rates and less polymer leading to a thinner polymer layer to hold on to particles. These results provide a better understanding of the binder behavior and its influence on the particle transfer process which opens-up the possibility of particle sorting process from a polydisperse suspension mixture and high-yield material transfer for a porous structure joining process. Additionally, the work demonstrates that by using higher MW polymers less polymer is needed to achieve the same results, which could lead to cost savings for coatings. Understanding the particle transfer process can also openup the reverse engineering of the liquid carrier system for a complex mixture, which can be beneficial for industrial applications including blood analysis, wastewater treatment, and others.

Declaration of competing interest

The authors declare that they have no known competing financial interests or personal relationships that could have appeared to influence the work reported in this paper.

Data availability

Data will be made available on request.

Acknowledgements

Financial supports from Grant NSF-CMMI # 2101751 and US-DOT # 693JK31850009CAAP are acknowledged. Author also like to acknowledge the NU-UMaine Seed grant for this work.

References

- [1] S.F. Kistler, P. Schweizer, LiquidFilm Coating: Scientific Principles and Their Technological Implications, 1997.
- [2] S.J. Weinstein, K.J. Ruschak, Coating flows, Annu. Rev. Fluid Mech. 36 (1) (2004) 29–53.
- [3] B. Khoda, A.M.M.N. Ahsan, S.M.N. Shovon, Dip coating from density mismatching mixture, J. Micro Nano-Manuf. 9 (2) (2021).
- [4] P. Chowdhury, et al., An approach for in situ measurement of anode temperature during the growth of self-ordered nanoporous anodic alumina thin films: influence of joule heating on pore microstructure, Electrochim. Acta 115 (2014) 657–664.
- [5] M. Sobhanimatin, S. Pourmahdian, M. Tehranchi, Fast inverse opal humidity sensor based on acrylamide/AMPS hydrogel, Mater. Today Commun. 26 (2021), 101997.

- [6] W. Li, et al., A hydrogel microsphere-based sensor for dual and highly selective detection of Al3+ and Hg2+, Sensors Actuators B Chem. 321 (2020), 128490.
- [7] D. Liu, et al., Milling force monitoring with thin-film sensors integrated into fixtures, Int. J. Adv. Manuf. Technol. 103 (1) (2019) 1519–1527.
- [8] D. Gallez, W.T. Coakley, Far-from-equilibrium phenomena in bioadhesion processes, Heterog. Chem. Rev. 3 (4) (1996) 443–475.
- [9] I. Khalil, B. Khoda, Sorting of poly-disperse particle by entrapment using liquid carrier system, J. Manuf. Sci. Eng. 144 (5) (2021).
- [10] B.M. Dincau, et al., Capillary sorting of particles by dip coating, Physical Review Applied 12 (1) (2019), 011001-011001.
- [11] K.S. Nanjundaswamy, et al., Electrode fabrication for Li-ion: processing, formulations and defects during coating, in: IECEC-97 Proceedings of the Thirtysecond Intersociety Energy Conversion Engineering Conference (Cat. No. 97CH6203), IEEE, 1997.
- [12] T. Steenberg, et al., Roll-to-roll coated PBI membranes for high temperature PEM fuel cells, Energy Environ. Sci. 5 (3) (2012) 6076–6080.
- [13] J.H. Burroughes, et al., Light-emitting diodes based on conjugated polymers, Nature 347 (6293) (1990) 539–541.
- [14] H.-L. Chou, S.-Y. Hsu, P.-K. Wei, Light emission in phase separated conjugated and non-conjugated polymer blends, Polymer 46 (13) (2005) 4967–4970.
- [15] D.E. Mentley, State of flat-panel display technology and future trends, Proceedings of the IEEE 90 (4) (2002) 453–459.
- [16] V.P. Elanjeitsenni, K.S. Vadivu, B.M. Prasanth, A review on thin films, conducting polymers as sensor devices, Mater. Res. Express 9 (2) (2022), 022001.
- [17] D. Braun, A.J. Heeger, Visible light emission from semiconducting polymer diodes, Appl. Phys. Lett. 58 (18) (1991) 1982–1984.
- [18] J. Kim, R. Friend, F. Cacialli, Improved operational stability of polyfluorene-based organic light-emitting diodes with plasma-treated indium—tin—oxide anodes, Appl. Phys. Lett. 74 (21) (1999) 3084–3086.
- [19] C. Wu, et al., Surface modification of indium tin oxide by plasma treatment: an effective method to improve the efficiency, brightness, and reliability of organic light emitting devices, Appl. Phys. Lett. 70 (11) (1997) 1348–1350.
- [20] M.S. Chebil, et al., Influence of outer-layer finite-size effects on the dewetting dynamics of a thin polymer film embedded in an immiscible matrix, Soft Matter 14 (30) (2018) 6256–6263.
- [21] C.E. Murphy, et al., Wire-bar coating of semiconducting polythiophene/insulating polyethylene blend thin films for organic transistors, J. Appl. Phys. 110 (9) (2011), 093523.
- [22] L.E. Scriven, Physics and applications of DIP coating and spin coating, MRS Proc. (1988) 121.
- [23] B. Levich, L. Landau, Dragging of a liquid by a moving plate, Acta Physicochim. URSS 17 (1942) 42.
- [24] B. Derjaguin, A. Titievskaya, Experimental study of liquid film thickness left on a solid wall after receeding meniscus, Dokl. Akad. Nauk USSR. 50 (1945) 307–310.
- [25] A. Gans, et al., Dip-coating of suspensions, Soft Matter 15 (2) (2019) 252–261.
- [26] F. Goucher, H. Ward, A problem in viscosity, Philos. Mag. 44 (6) (1922) 1002.
 [27] D. Quéré, Fluid coating on a fiber, Annu. Rev. Fluid Mech. 31 (1) (1999) 347–384.
- [28] D.A. White, J.A. Tallmadge, A theory of withdrawal of cylinders from liquid baths, AIChE J. 12 (2) (1966) 333–339.
- [29] F. Deng, Q.-K. Nguyen, P. Zhang, Multifunctional liquid metal lattice materials through hybrid design and manufacturing, Addit. Manuf. 33 (2020), 101117.
- [30] S.M.N. Shovon, et al., Micro-particle entrainment from density mismatched liquid carrier system, Sci. Rep. 12 (1) (2022) 9806.
- [31] K.J. Ruschak, Coating flows, Annu. Rev. Fluid Mech. 17 (1) (1985) 65-89.
- [32] C.E. Colosqui, J.F. Morris, H.A. Stone, Hydrodynamically driven colloidal assembly in dip coating, Phys. Rev. Lett. 110 (18) (2013), 188302.
- [33] A. Sauret, et al., Capillary filtering of particles during dip coating, Phys. Rev. Fluids 4 (5) (2019), 054303.
- [34] B.M. Dincau, et al., Entrainment Particles During the Withdrawal of a Fiber From a Dilute Suspension, 2020.
- [35] M. Faustini, et al., Preparation of Sol—Gel films by dip-coating in extreme conditions, J. Phys. Chem. C 114 (17) (2010) 7637–7645.
- [36] S. Mueller, E.W. Llewellin, H.M. Mader, The rheology of suspensions of solid particles, Proceedings of the Royal Society A: Mathematical, Physical and Engineering Sciences 466 (2116) (2010) 1201–1228.
- [37] S. Dhar, S. Chattopadhyay, S. Majumdar, Signature of jamming under steady shear in dense particulate suspensions, J. Phys. Condens. Matter 32 (12) (2019), 124002.
- [38] S. Palma, H. Lhuissier, Dip-coating with a particulate suspension, J. Fluid Mech. 869 (2019) R3.
- [39] Y. Wang, et al., Large-areaSelf Assembled Monolayers of Silica Microspheres Formed by Dip Coating, TEXAS UNIV AT ARLINGTON DEPT OF ELECTRICAL ENGINEERING, 2010.
- [40] A.W. Adamson, A.P. Gast, Physical Chemistry of Surfaces 15, Interscience publishers, New York, 1967.
- [41] H.J. Ploehn, W.B. Russel, Interactions between colloidal particles and soluble polymers, in: Advances in Chemical Engineering, Elsevier, 1990, pp. 137–228.
- [42] P. Yimsiri, M.R. Mackley, Spin and dip coating of light-emitting polymer solutions: matching experiment with modelling, Chem. Eng. Sci. 61 (11) (2006) 3496–3505.
- [43] C.E. Federico, et al., Large strain/time dependent mechanical behaviour of PMMAs of different chain architectures. Application of time-temperature superposition principle, Polymer (2018) 139.
- [44] A.I. Alam, Additively manufactured metal and polymer lattice structures with eulerian paths, in: MS Thesis, Mechanical Engineering Department, University of Maine, 2022
- $\hbox{\bf [45]}\ \ \hbox{I. Teraoka, PolymerSolutions: An Introduction to Physical Properties, 2002.}$

- [46] M.V.S. Rao, Viscosity of dilute to moderately concentrated polymer solutions, Polymer 34 (3) (1993) 592–596.
- [47] P. Geng, A. Zore, M.R. Van De Mark, Investigation of the evaporation rate of water from colloidal unimolecular polymer (CUP) systems by isothermal TGA, Polymers 12 (11) (2020) 2752.
- [48] D. Gilbert, R. Valette, E. Lemaire, Impact of particle stiffness on shear-thinning of non-Brownian suspensions, J. Rheol. 66 (1) (2022) 161–176.
- [49] R. Pasquino, et al., Rheology of dilute and semidilute noncolloidal hard sphere suspensions, J. Rheol. 52 (6) (2008) 1369–1384.
- [50] J. Duffy, Measuring the Rheology of Polymer Solutions, Malvern Instruments Limited, 2015.
- [51] M.L. Huggins, The viscosity of dilute solutions of long-chain molecules. IV. Dependence on concentration, J. Am. Chem. Soc. 64 (11) (1942) 2716–2718.